Exploring GPCR-arrestin interfaces with genetically encoded crosslinkers

Thore Böttke[1] [ID], Stefan Ernicke[1], Robert Serfling[1], Christian Ihling[2], Edyta Burda[3],
Vsevolod V Gurevich[4] [ID], Andrea Sinz[2] & Irene Coin[1,*] [ID]

Abstract

β-arrestins (βarr1 and βarr2) are ubiquitous regulators of G protein-coupled receptor (GPCR) signaling. Available data suggest that β-arrestins dock to different receptors in different ways. However, the structural characterization of GPCR-arrestin complexes is challenging and alternative approaches to study GPCR-arrestin complexes are needed. Here, starting from the finger loop as a major site for the interaction of arrestins with GPCRs, we genetically incorporate non-canonical amino acids for photo- and chemical crosslinking into βarr1 and βarr2 and explore binding topologies to GPCRs forming either stable or transient complexes with arrestins: the vasopressin receptor 2 (rhodopsin-like), the corticotropin-releasing factor receptor 1, and the parathyroid hormone receptor 1 (both secretin-like). We show that each receptor leaves a unique footprint on arrestins, whereas the two β-arrestins yield quite similar crosslinking patterns. Furthermore, we show that the method allows defining the orientation of arrestin with respect to the GPCR. Finally, we provide direct evidence for the formation of arrestin oligomers in the cell.

Introduction

Arrestins are a small family of highly homologous cytosolic proteins that dock to activated and phosphorylated G protein-coupled receptors (GPCRs) to desensitize G protein-mediated signaling (Gurevich, 2014; Shukla & Dwivedi-Agnihotri, 2020). Four arrestin isoforms are expressed in vertebrates: Two quench the signaling by rhodopsin (Rho) and cone opsins in the retina (arr1 and arr4, also called

"visual" arrestins), whereas the other two serve ubiquitously the hundreds of non-visual GPCRs encoded in the human genome (arr2 and arr3, a.k.a. βarr1 and βarr2, called "non-visual" or β-arrestins). All arrestins in their basal state consist of β-sheets organized in two cup-like domains (N- and C-domain) with four exposed loops in the central crest of the receptor binding side (Fig 1A). The *finger loop* shares a consensus motif with the C-terminal helix of Gα from Gi/transducin and competes with it for the cavity that opens in the transmembrane (TM) core of active GPCRs (Szczepek et al, 2014). This loop is indispensable for the formation of a fully engaged arrestin–receptor complex (core conformation). Arrestin variants lacking the *finger loop* only bind to the phosphorylated GPCR C-terminal tail via their N-domain (tail conformation) (Shukla et al, 2014; Cahill et al, 2017; Nguyen et al, 2019). Moreover, the *finger loop* determines the binding preferences of arrestin to receptors (Vishnivetskiy et al, 2004, 2011; Chen et al, 2017).

G protein-coupled receptors are divided into two classes with respect to arrestin binding (Oakley et al, 1999, 2000; Luttrell & Lefkowitz, 2002). Class A receptors form transient and rapidly dissociating complexes with arrestin, and resensitize rapidly. These receptors interact with both β-arrestins, but show a bias toward βarr2. Besides the prototypical β2-adrenergic, class A receptors include, among others, the μ opioid, endothelin A, and dopamine D1A receptors (all rhodopsin-like GPCRs), as well as the corticotropin-releasing factor receptor (CRF1R, secretin-like) (Oakley et al, 2007; Grammatopoulos, 2012). Class B receptors form long-lived complexes with arrestin that remain stable through the internalization via clathrin-coated pits, and resensitize slowly. Class B receptors bind with high affinity either β-arrestin. The prototypic class B arrestin binder is the vasopressin 2 receptor (V2R). Other receptors forming stable complexes with arrestin include the angiotensin II type 1 receptor (AT1R), the oxytocin receptor, the neurotensin 1 receptor (NTS1R), and the secretin-like parathyroid hormone receptor (PTH1R) (Oakley et al, 2001; Vilardaga et al, 2002). The latter has been shown to form GPCR–arrestin–G protein megaplexes that mediate prolonged signaling after internalization in endosomes (Wehbi et al, 2013; Thomsen et al, 2016). A major determinant for the stability of GPCR-arrestin complexes is the
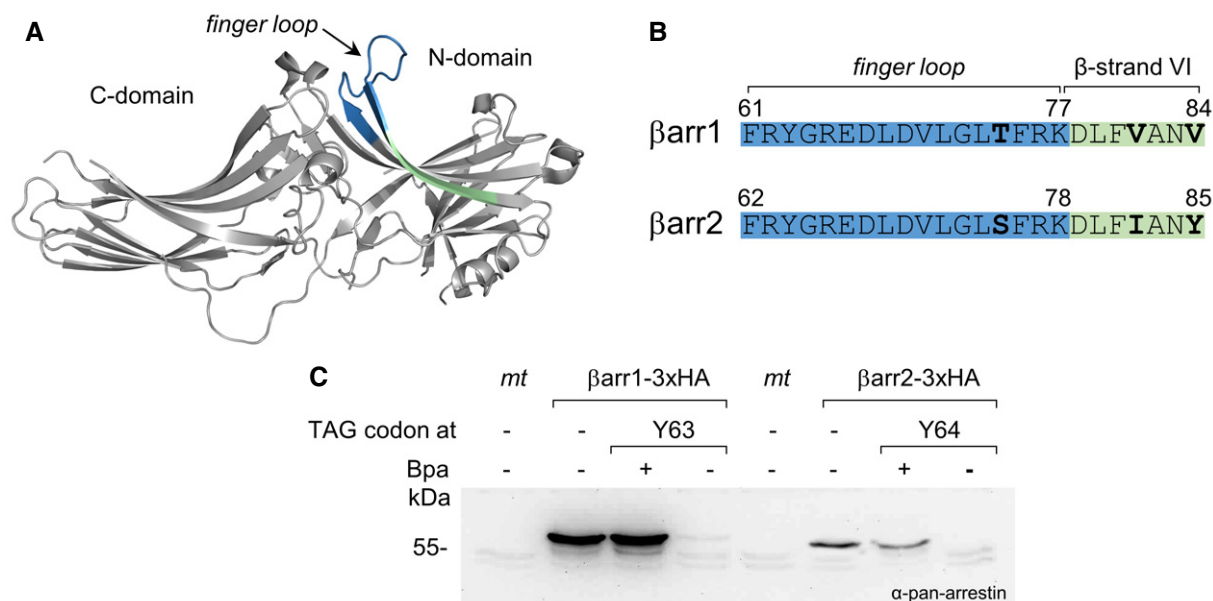
Figure 1. Genetic incorporation of Bpa into β-arrestins.

A Ribbon representation of bovine βarr1 (PDB 1G4M) (Han *et al*, 2001). The *finger loop* is highlighted in blue and β-strand VI in pale green.
B Sequence alignment of the *finger loop* and N-terminal part of β-strand VI in bovine β-arrestins, color coded as in (A). Divergent positions are shown in bold.
C Western blots of the lysates of HEK293T cells, resolved on SDS–PAGE and stained with a pan-arrestin antibody. *mt*, mock transfected. Bpa: benzoyl-phenylalanine. Arrestins were equipped with a 3xHA tag at the C-terminus, which increases their size of about 3 kDa compared to the endogenous proteins (βarr1 47 kDa, βarr2 46 kDa). βarr1 and βarr2 were transfected at 1/3 DNA compared to the corresponding TAG-mutants.

C-terminal tail of the receptor. In general, GPCRs carrying clusters of Set/Thr in the C-terminal tail show a class B behavior (Oakley *et al*, 1999).

Overall, GPCR-arrestin complexes are highly dynamic and the biophysical determination of their structure is technically very challenging. To date, only a few 3D structures of arrestin–GPCR complexes have been solved: the crystal structure of the rhodopsin (Rho)-bound arr1 (Kang *et al*, 2015; Zhou *et al*, 2017), and the three very recent cryo-electron microscopy (cryo-EM) structures of βarr1 in complex with the class B NTS_1R (Yin *et al*, 2019; Huang *et al*, 2020), the muscarinic acetylcholine-2-receptor (M_2R) (Staus *et al*, 2020), and the $β_1$-adrenoceptor ($β_1$-AR) (Lee *et al*, 2020). The $β_1$-AR belongs to class A arrestin binders (Shiina *et al*, 2000, Eichel *et al*, 2016), whereas contradictory findings have been reported for the M_2R (Gurevich *et al*, 1995, Jones *et al*, 2006).

As expected on the basis of numerous biochemical studies (reviewed in (Gurevich & Gurevich, 2006)), the existing structures confirm that βarr1 can assume distinct orientations depending on which receptor it binds to. Likewise, position and conformation of the *finger loop* differ between the complexes. Moreover, the binding mode of arrestin to the same GPCR can be affected by specific phosphorylation patterns, which lead to different downstream responses (barcode hypothesis) (Tobin *et al*, 2008; Nobles *et al*, 2011; Yang *et al*, 2015; Zhou *et al*, 2017; Mayer *et al*, 2019; Kaya *et al*, 2020). These facts, together with the observation that there are no conserved motifs in the intracellular part of the GPCRs, suggest that homology models based on the few available structures likely have limited predictive value. In addition, the lipid environment has been shown to affect the conformation of isolated GPCR-arrestin

complexes (Staus *et al*, 2020). It is also worth mentioning that the structures of M_2R and $β_1$-AR could only be achieved by equipping the receptors with the C-terminal tail of the V_2R, a modification that stabilizes the GPCR-arrestin complexes by transforming class A arrestin binders into class B ones (Oakley *et al*, 2000). Methods are needed both to address complexes that elude direct structural characterization and to validate biophysical data in the living cell.

We have a long experience in the application of genetically encoded chemical tools to map interactions of GPCRs with their ligands (Coin *et al*, 2011, 2013; Seidel *et al*, 2017), as well as interactions of nuclear receptors (Schwarz *et al*, 2013, 2016). Here we show that the incorporation of crosslinking non-canonical amino acids (ncAAs) into arrestins allows the comparison of the topology of GPCR-arrestin complexes in intact cells.

Results and Discussion

We selected 24 positions in βarr1 and βarr2 covering the finger loop italic and the N-terminal segment of the following β-strand (Fig 1B). The codons of each amino acid along this stretch were substituted with the amber stop codon TAG for the incorporation of the photo-activatable ncAA benzoyl-Phe (Bpa). A preliminary test on a pair of homologous βarr1/βarr2 mutants showed that Bpa was smoothly incorporated into both arrestins via amber suppression (Wang, 2017a; Lang *et al*, 2018), with minimal read-through occurring in the absence of the ncAA (Fig 1C). Transfected arrestins were expressed in very large excess compared to the endogenous counterparts. βarr1 is known to express at a higher level than βarr2 in
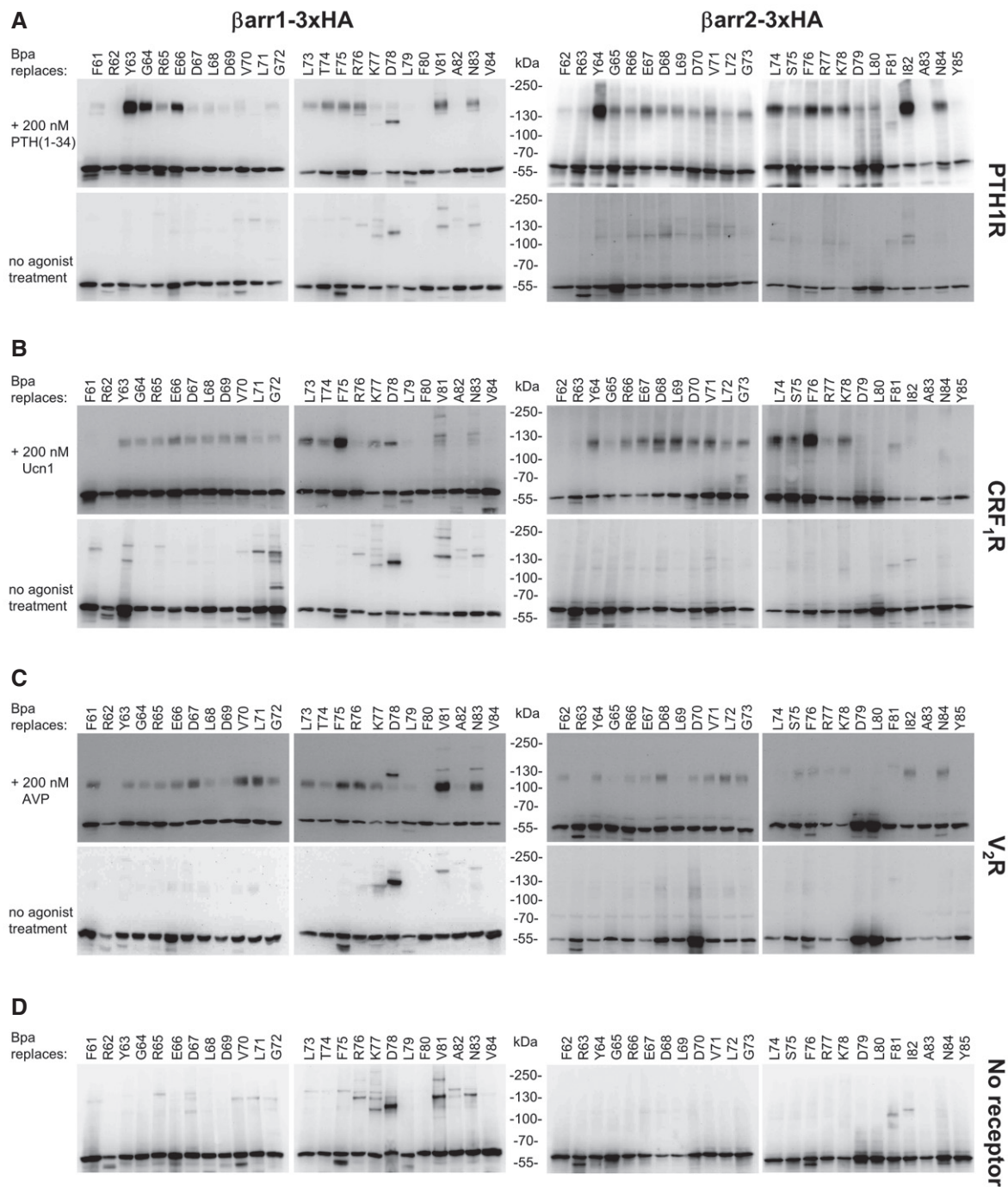
Figure 2. Photo-crosslinking of Bpa-arrestins with three different GPCRs with and without agonist stimulation.

Each panel represents immunoblots of whole cell lysates stained with an anti-HA antibody detecting arrestin. In the left panels, GPCRs were combined with βarr1 variants and in the right panels with βarr2 variants. Residues replaced by Bpa are indicated above each lane. Covalent arrestin–receptor complexes are expected between 100–200 kDa, considering the size of the receptors (V_2R 41.5 kDa, PTH1R 63.8 kDa, CRF_1R, 46.3 kDa) and their glycosylation.

A PTH1R, agonist PTH(1–34).
B CRF_1R, agonist Urocortin 1 (Ucn1).
C V_2R, agonist arginine-vasopressin (AVP).
D No receptor.

native cells and different cell lines (Gurevich *et al*, 2004; Coffa *et al*, 2011). This can be observed also here, both in the case of endogenous arrestins and the Bpa-mutants, which expressed at a homogenous yield (Fig 2). The Bpa-mutation did not hamper the recruitment of either arrestin to the PTH1R receptor, suggesting that the overall functionality of the arrestins is preserved (Appendix Fig S1).

The two sets of Bpa-βarr1 and Bpa-βarr2 were combined with GPCRs forming either stable (class B) or transient (class A) complexes with arrestins. We selected two class B receptors belonging to two distinct phylogenetic GPCR families, the V_2R (rhodopsin-like) and the PTH1R (secretin-like), as well as the class A receptor CRF_1R (secretin-like). The latter was preferred to other class A GPCRs because the CRF system is well established in our laboratory. Photo-crosslinking experiments were carried out in live HEK293T cells expressing one receptor and one arrestin variant, for a total of 144 combinations, with or without agonist stimulation (Fig EV1). Cell lysates were resolved on SDS–PAGE and immunoblotted with antibodies detecting either arrestin (Fig 2) or the GPCR (Fig EV2). For a subset of arrestin–receptor combinations, high molecular weight (MW) bands were observed (Fig 2A–C upper panels). Most bands appeared only when arrestin recruitment was triggered by the agonist treatment, but were not visible when the receptor was not activated (Fig 2A–C, lower panels) or absent (Fig 2D). The apparent MW was receptor-dependent and was reduced by deglycosylation (Fig 3). These activation-dependent bands were therefore attributed to covalently crosslinked receptor–arrestin complexes. The crosslinking patterns differed substantially between the different receptors, whereas the strongest bands with the same receptor appeared at homologous Bpa positions in the two arrestins. The most prominent bands were obtained with Bpa63/64-βarr1/2 (crosslinker at the beginning of the *finger loop*) with the PTH1R, Bpa75/76-βarr1/2 (crosslinker at the C-terminal portion of the *finger loop*) with the CRF_1R and Bpa81/82-βarr1/2 (crosslinker in β-strand VI) with the V_2R. Overall, these results suggest specific binding modes of arrestins at different receptors, whereas the two arrestins appear to bind to each receptor in a similar fashion.

These findings confirm the observation from the 3D structures, which show distinct binding modes of βarr1 to the different receptors. In a recent report, photo-crosslinkers genetically incorporated into the intracellular domains of the AT_1R have revealed distinct binding modalities of AT_1R to βarr1 depending on the type of the agonist used for its activation (natural angiotensin vs. arrestin-biased AT_1R ligands) (Gagnon *et al*, 2019). Collectively, these results demonstrate that genetically encoded photo-crosslinkers incorporated either into a GPCR or into arrestin allow elucidating with a good sensitivity differences in the arrangement of arrestin–GPCR complexes.

Other crosslinking bands observed in our experiments appeared independently from activation of a GPCR. The most prominent activation-independent bands were observed with Bpa78- and Bpa81-βarr1 at apparent MW ~ 120 kDa. They appeared in all analyses (Fig 2A–C) even in the absence of a co-transfected receptor (Fig 2D) and were not affected by deglycosylation (Fig 3). Only very faint bands were observed with the Bpa-βarr2 set.

To identify the nature of these crosslinking products, Bpa78-βarr1 was equipped with a 2xStrep tag at the C-terminus, expressed in large scale in HEK293T cells, and isolated via the Strep-Tactin® XT system either before or after UV irradiation (Appendix Fig S2A). As shown in Fig 4, the crosslinking product obtained by *in vitro* irradiation of the isolated Bap78-βarr1 runs exactly as the crosslinking product obtained when irradiating the intact cells (Fig 4A). Furthermore, the crosslinked samples were subjected to size exclusion chromatography (SEC), yielding two partially resolved major peaks (Fig 4B). Eluates were analyzed by immunoblotting (Fig 4C) and by MALDI mass spectrometry (MS, Fig 4D). The peak at higher retention volume (V_R3) yielded a single signal in Western blot and a whole-protein mass spectrum compatible with a βarr1 monomer (50.4 kDa). The other eluted fraction (V_R2) contained a mixture of βarr1 with the crosslinking product, and featured in MS a further signal at double mass. Furthermore, SEC fractions were enzymatically digested and applied to nano-HPLC/nano-ESI-Orbitrap-MS/MS. In the SEC fraction containing the crosslinked product, βarr1 was identified as the by far most abundant protein with sequence
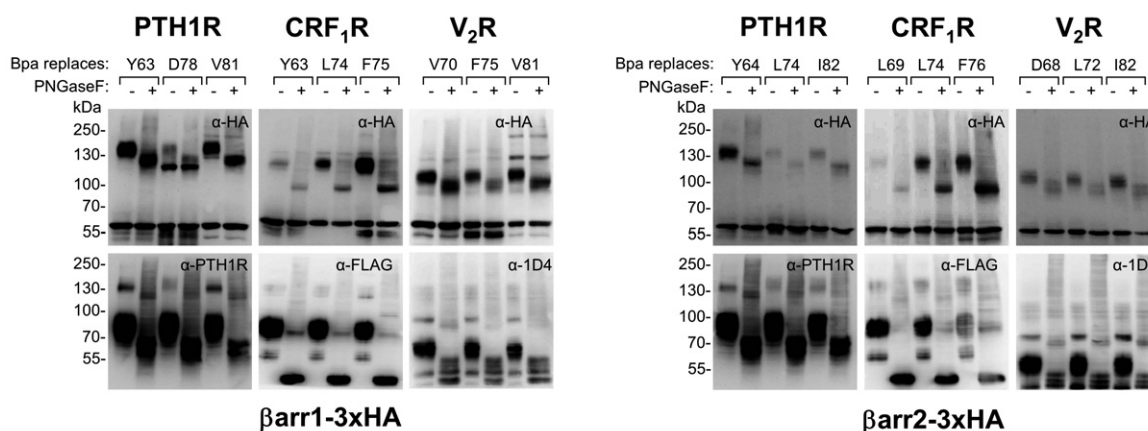
Figure 3. Response of photo-crosslinked samples to deglycosylation.
Aliquots from agonist-treated samples shown in Fig 2 were deglycosylated with PNGaseF, run on SDS–PAGE and immunoblotted with antibodies detecting arrestin (upper panels, α-HA) and the GPCRs (as indicated, CRF_1R is equipped with a N-terminal FLAG, V_2R carries a C-terminal 1D4 epitope).
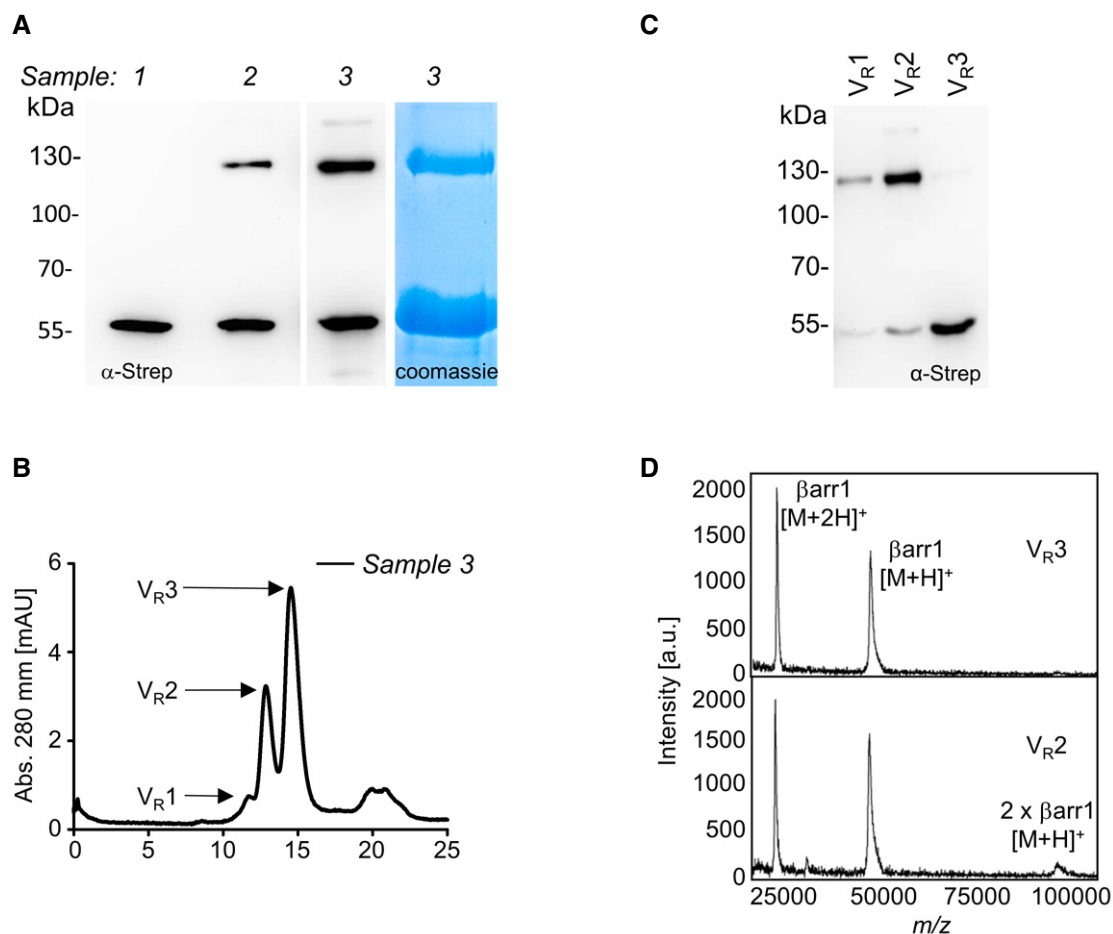
Figure 4. Analysis of activation-independent crosslinking band at D78Bpa-βarr1.

A SDS–PAGE and immunoblots of immunoprecipitated samples. Sample 1 was immunoprecipitated without previous UV treatment. Sample 2 is the product of irradiation of sample 1. Sample 3 was treated with UV light before immunoprecipitation. All samples were run in parallel on the same gel.

B Size exclusion chromatography (SEC) of Sample 3.

C Western blot of the fractions eluted by SEC.

D MALDI-TOF analysis of the SEC fractions V_R2 and V_R3. The spectrum of sample V_R2 shows a $[M + H]^+$ peak featuring twice the mass (~ 108,000 Da) of the $[M + H]^+$ peak of the βarr1 monomer (sample V_R3, ~ 50,400 Da).

coverage of 90% (Appendix Fig S2B) and 1,951 PSMs (peptide spectral matches) compared to only 22 PSMs for the second most abundant protein. Collectively, the results identify this crosslinking product as a covalent βarr1 dimer.

β-arrestins are known to self-associate in solution (Hanson *et al*, 2008; Chen *et al*, 2014), as well as in crystals and in cells (Han *et al*, 2001; Milano *et al*, 2006; Boularan *et al*, 2007; Zhan *et al*, 2011). Our results support the notion that β-strand VI participates in the βarr1 association interface, which is in line with the current oligomerization model of this arrestin. On the other hand, it cannot be excluded that at least some of the weak activation-independent crosslinking signals at high MW belong to complexes of arrestin with endogenous proteins. Both arrestins are known to function as scaffolds for a wide variety of proteins, with the most prominent examples being kinases like ERKs, JNK3, or other MAPKs (Xiao *et al*, 2007; Song *et al*, 2009), as well as proteins involved in GPCR trafficking, such as clathrin and AP2 (Goodman *et al*, 1996; Laporte

et al, 1999). Elucidation of the nature of all receptor-independent crosslinking signals awaits further experiments.

Other receptor-independent bands were visible below the apparent MW of arrestin itself (e.g., Bpa75/76-βarr1/2; Fig 2). Position 75/76 is quite intriguing, because Bpa75/76-βarr1/2 give both a low-MW band and an activation-dependent crosslinking band (especially with CRF_1R, Fig 2). To test whether low-MW bands are due to intra-molecular crosslinking, we applied proximity-induced pairwise crosslinking (Fig 5A) (Xiang *et al*, 2013; Wang, 2017b; Coin, 2018; Seidel *et al*, 2019). The mildly electrophilic ncAA O-(2-bromoethyl)-tyrosine (BrEtY) (Xiang *et al*, 2014) was genetically incorporated at position F75 of βarr1. Simultaneously, F244, which lies in its close proximity in the inactive βarr1 (Fig 5B, left), was mutated to Cys. Indeed, BrEtY75-Cys244-βarr1, but not BrEtY75-βarr1, yielded on Western blot a major band at the exact position of the receptor-independent product generated by UV irradiation of Bpa75-βarr1 (Fig 5C). When arrestin is activated, the *finger loop*
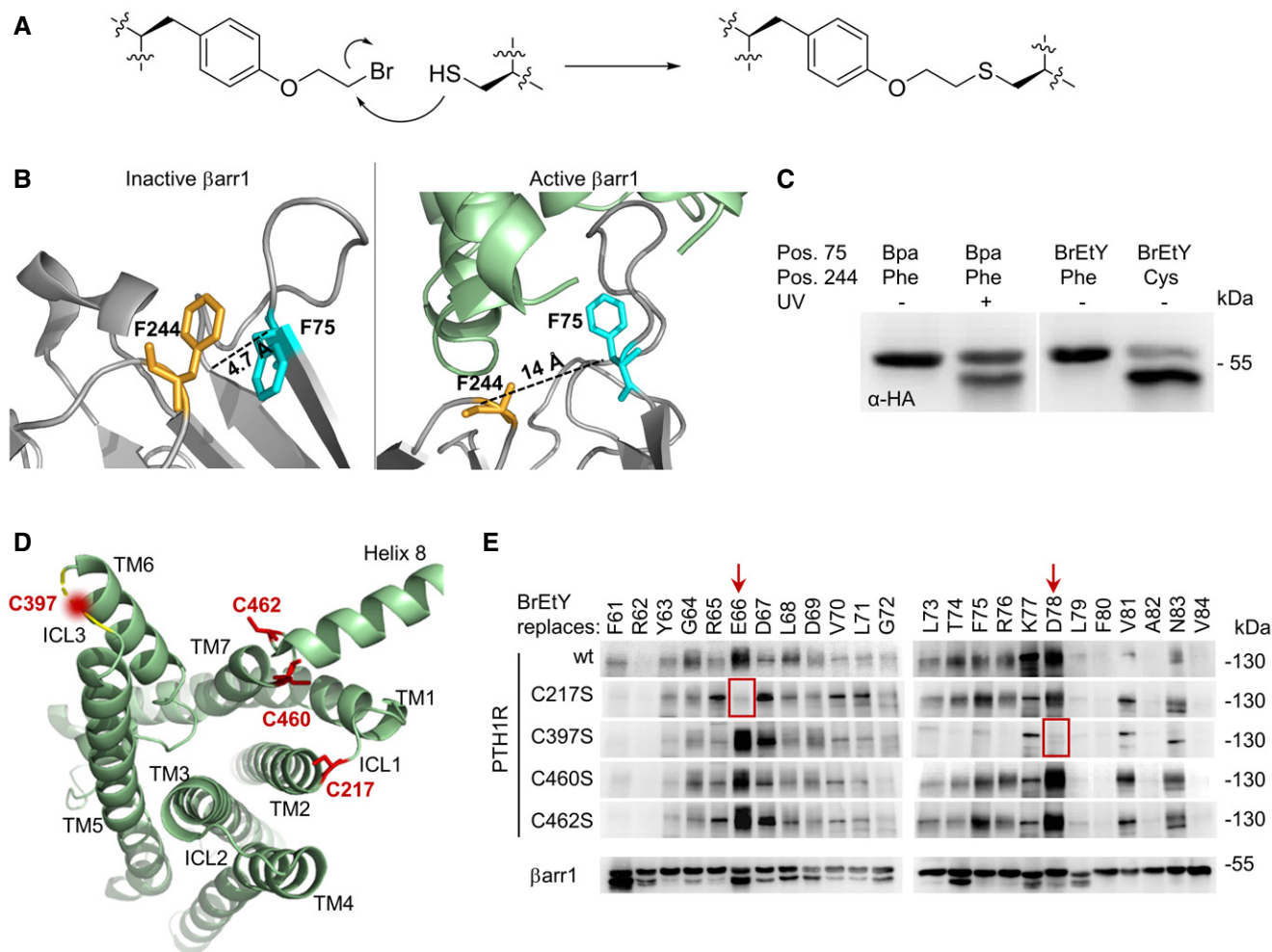
Figure 5. Proximity-induced pair-wise crosslinking.

A   Mechanism of the nucleophilic substitution reaction between BrEtY and Cys. The product is a thioether, which is stable in reducing SDS–PAGE.

B   Ribbon representation of inactive (PDB 1G4M (Han *et al*, 2001)) and active (PDB 6U1N (Staus *et al*, 2020)) βarr1. Arrestin is in gray and M₂R in pale green.

C   Western blot of whole cell lysates from HEK293T cells expressing βarr1 mutated as indicated in the top lines. All samples were run in parallel on the same gel.

D, E   Pair-wise crosslinking between BrEtY-βarr1-3xHA and wt PTH1R. (D) Ribbon representation of active PTH1R as seen from the intracellular side (PDB 6NBF) (Zhao *et al*, 2019). Cys residues are shown in red. ECL3 (not resolved in the structure) is represented as a yellow dashed line. The approximate position of the Cys residue in this loop is marked with a fuzzy red circle. (E) Western blot of whole cells lysates stained with an α-HA antibody. Residues of βArr1 exchanged with BrEtY are indicated in the upper row, and mutations at PTH1R are indicated on the left side. The red arrows indicate the two most prominent signals. Red squares indicate signals that vanish upon removal of specific Cys residues in PTH1R.

moves away from F244 to insert into the receptor TM cavity (Fig 5B, right), so that Bpa at position 75 can capture the receptor. Thus, the photo-crosslinking data reveal the co-existence of two distinct populations of arrestins in our experiments: a receptor-engaged population and an inactive population in basal conformation. The result is not surprising, as especially βarr1 is largely overexpressed.

We further explored whether chemical crosslinking can be applied to determine inter-molecular receptor-arrestin proximity points, as it was shown to capture protein–protein interactions in live cells (Yang *et al*, 2017). The PTH1R contains four Cys residues in the juxtamembrane region at the cytosolic side (Fig 5D). To investigate whether any of these residues lie close to the *finger loop* of the associated arrestin, we incorporated BrEtY in the same 24

positions of βarr1 previously substituted with Bpa. BrEtY-βarr1 mutants were co-expressed with PTH1R in HEK293T cells, and arrestin recruitment was triggered by agonist activation. Strong arrestin–receptor crosslinking was detected when BrEtY was incorporated at position E66 and D78, along with some minor signals (Fig 5E). To investigate which Cys reacted with which BrEtY, the four Cys in PTH1R where mutated one by one into Ser and Ser-PTH1R mutants were combined with the same BrEtY-βarr1 set. Crosslinking obtained with BrEtY66- and BrEtY78-βarr1 selectively disappeared upon removal of C217 and C397, respectively (Fig 5E). Overall, the results of chemical crosslinking suggest that in the PTH1R-βarr1 complex, the N-terminal portion of the *finger loop* (E66) points toward ICL1 (C217) of the receptor, whereas the C-

terminal segment (T74-K77, weaker crosslinking signals) up to the beginning of β-strand VI (D78) is proximal to ICL3 (C397). This is compatible with the orientation observed in the arr1-Rho and the βarr1-M_2R complex, but not the βarr1-NTS_1R (Fig EV3). This result clearly confirms the observation from the existing structures that the orientation of arrestin on the receptor does not determine whether the GPCR–arrestin complexes are stable or transient.

In conclusion, we have devised a biochemical method to investigate topologies of arrestin binding to GPCRs in intact cells, which exploits the genetic incorporation of photo-activatable and mildly electrophilic ncAAs into arrestin for photo- and chemical crosslinking experiments. In the first instance, photo-crosslinking enables distinguishing footprints of different receptors on the same arrestin. We show that different footprints are not related to the phylogenetic class of the investigated GPCRs (rhodopsin-like vs. secretin-like) nor to the type of interaction with arrestin (transient or stable), but are indeed specific for individual GPCRs. The similar footprints obtained on βarr1 and βarr2 suggest a common binding mode for the two arrestins. In the second instance, chemical crosslinking reveals inter-molecular pairs of amino acids coming into proximity in the GPCR-arrestin complex. By exploiting the presence of natural Cys residues in PTH1R, we have defined the orientation of the *finger loop* in the intracellular crevice of the active receptor. We anticipate that the incorporation of BrEtY into arrestins combined with Cys-mutagenesis of the GPCR will allow the detailed investigation of whole GPCR–arrestin interfaces. Overall, once a large set of TAG-arrestin mutants is generated, the method ideally lends itself to the comparison of arrestin binding to several receptors in a short time. We have shown that the approach is applicable both to stable and transient arrestin–receptor complexes, which provides a unique possibility for investigating interactions of arrestin with class A GPCRs without the need of generating chimeras with altered binding behavior. Last, but not least, ncAA-crosslinking provides information directly from the cellular environment, which cannot be obtained by crystallography or cryo-EM.

Materials and Methods

Molecular biology

Cloning was performed in *Escherichia coli* DH5α. All PCRs were run with Phusion High Fidelity Polymerase. The ORFs of all arrestins and receptors were cloned into pcDNA3.1 (Thermo Fisher Scientific) using standard cloning methods. Sequences for N- or C-terminal affinity tags were built from scratch using overlapping primers. The primers for the systematic TAG mutagenesis of βarr1 and βarr2 were designed with AA scan (Sun *et al*, 2013), and all changes were made using site directed mutagenesis. Oligonucleotides were purchased by Microsynth (Balgach, CH) and Biomers (Ulm, DE). All sequences were verified by Sanger sequencing (Seqlab Göttingen, DE).

Plasmids for ncAA incorporation (Appendix Fig S3)

pIRE4-Bpa (available from ADDGENE #155342)

Plasmid pIRE4-BpaRS is a bicistronic construct built exactly as pIRE4-Azi (Seidel *et al*, 2017; Serfling *et al*, 2018a). The backbone is originally based on pEGFP-N1 (Clontech, Mountain View, CA) and bears a Kan/Neo resistance. The CMV-EGFP sequence of pEGFP-N1 was substituted with the AARS cassette, followed by the tRNA cassettes immediately downstream of the polyadenylation sequence. pIRE4-Bpa contains a humanized gene of the *E. coli* BpaRS (Chin *et al*, 2003) (custom synthesized by GeneArt, Thermo Fisher Scientific) under control of a PGK promoter and four tandem repeats of a cassette for the expression of the tRNA suppressor from the *Bacillus stearothermophilus* tRNA^{Tyr} (*Bst*Yam), including a U6 promoter and a 5′-trailer.

pNEU-MmXYRS-4xM15 (available from ADDGENE #155343)

pNEU-MmXYRS-4xM15 is a bicistronic vector. The pNEU backbone is essentially the same as pcDNA3.1 with some variations in the restriction sites. The plasmid contains a humanized gene for the XYPylRS that recognizes BrEtY (Xiang *et al*, 2014) derived from *Methanosarcina mazei* PylRS (custom synthesized by GeneArt) under control of a CMV promoter, as well as four tandem repeats of the gene encoding for the enhanced pyrrolysine-tRNA^{M15} (Serfling *et al*, 2018a). The tRNA gene is depleted of the CCA end and is driven by a U6 promoter and followed by a T-rich trailer.

Cell culture

HEK293T cells were maintained in Dulbecco's modified Eagle's medium (DMEM; high glucose 4.5 g/l, 4 mM glutamine, pyruvate; Thermo Fisher Scientific) supplemented with 10% fetal calf serum (FCS; v/v; Thermo Fisher Scientific) and 100 U/ml penicillin and 100 μg/ml streptomycin (Thermo Fisher Scientific) (full DMEM) at 37°C under 5% CO_2 and 95% humidity. Cells were passaged at ~ 70–80% confluence.

Photo-crosslinking experiments (Fig EV1)

HEK293T cells were seeded at 500,000 cells per well in six-well plates in 2 ml full DMEM. After 24 h, the media was exchanged with full DMEM supplemented with 250 μM *p*-benzoyl-phenylalanine (Bachem). Cells were transfected using PEI (Polysciences) at a ratio of PEI:DNA 3:1 (w/w) in lactate buffered saline (20 mM sodium lactate pH 4 and 150 mM NaCl) (Serfling & Coin, 2016; Serfling *et al*, 2018b). Cells were co-transfected with three plasmids: (i) 900 ng of a plasmid bearing the arrestin stop codon mutant, (ii) 900 ng of pIRE4-BpaRS, and (iii) 300 ng of a vector encoding the GPCR. Forty-eight hours post-transfection, the media was aspirated and exchanged with 1 ml activation buffer (PBS + 0.1% BSA). For the stimulation of the cells, the activation buffer was supplemented with 200 nM of the corresponding agonist (Ucn1 for CRF_1R, AVP for V_2R and PTH(1–34) for PTH1R). After 15 min at 37°C, the cells were irradiated with UV light for 15 min in a BLX-365 crosslinker (Bio-Budget Technologies, 365 nm; 4 × 8 W bulbs). Then, the activation buffer was aspirated and the cells were put at −80°C for 20–30 min, detached with 1 ml PBS supplemented with 1× protease inhibitor cocktail (Roche), and pelleted at 2,500 *g* for 10 min at 4°C. Cells were lysed in 80 μl Triton lysis buffer 1 (50 mM HEPES pH 7.5, 150 mM NaCl, 10% glycerol, 1% Triton X-100, 1.5 mM $MgCl_2$, 1 mM EGTA, 1 mM DTT and 1× protease inhibitor) for 30 min on ice and vortexed every 10 min. The samples were centrifuged at 16,000 *g* for 10 min at 4°C, and supernatants were transferred to pre-chilled tubes. For SDS–PAGE, 4 μl of supernatant was incubated for 30 min at 37°C in lithium dodecyl sulfate (LDS)-sample buffer

(250 mM Tris–HCl pH 8.5, 2% (w/v) LDS, 150 mM DTT, 0.4 mM EDTA, 10% (v/v) glycerol, and 0.2 mM Coomassie Brilliant Blue G). For deglycosylation, samples were treated with PNGaseF (New England Biolabs) according to the manufacturer's protocol and LDS-sample buffer was added before SDS–PAGE.

Chemical crosslinking experiments

HEK293T cells were seeded at 500,000 cells per well in six-well plates in full DMEM. After 24 h, the media was exchanged with full DMEM supplemented with 250 µM BrEtY (synthesized as described in Xiang et al (2014)). Cells were transfected using PEI as described above. Cells were co-transfected with three plasmids: (i) 900 ng of a plasmid bearing the arrestin stop codon mutant, (ii) 900 ng of pNEU-MmXYRS-4xM15, and (iii) 300 ng of a vector encoding for PTH1R or a Ser-PTH1R mutant. Forty-eight hours later, the media was aspirated and the cells were stimulated for 90 min with 1 ml activation buffer supplemented with 200 nM PTH(1–34). Cell lysis and sample preparation for SDS–PAGE were carried out as described in the section about photo-crosslinking.

SDS–PAGE and Western blot

Samples were resolved on 8% Tris/glycine polyacrylamide gels and transferred to a PDVF membrane (Millipore Immobilon, Merck, pore size 0.45 µm). The membranes were blocked by 5% non-fat dry milk powder (NFDM) in TBS-T (20 mM Tris–HCl pH 7.4, 150 mM NaCl and 0.1% (v/v) Tween-20) for at least 1 h at RT. Primary antibodies were diluted in 5 % NFDM in TBS-T as follows: α-HA-4D2 (Roche) 1:2,000; α-PTH1R 4D2 (Thermo Fisher Scientific) 1:2,000; α-FLAG-HRP M2 (Sigma-Aldrich) 1:5,000; α-1D4-HRP (Santa Cruz Biotechnology, sc-57432) 1:2,000. Membranes were incubated for either 1 h at RT (α-FLAG-HRP) or overnight at 4°C with the primary antibody (α-HA, α-PTH1R and α-1D4-HRP), followed by 3 × 10 min washes in TBS-T. Secondary antibodies, either α-rat-HRP (Cell Signaling) or α-mouse-HRP (Santa Cruz Biotechnology, sc-516102), were used at 1:10,000 in 5% NFDM in TBS-T for 1 h at RT followed by 3 × 10 min wash cycles in TBS-T. Membranes were soaked in homemade ECL reagent (10 parts 0.1 M Tris–HCl pH 8.6 with 250 mg/l luminol, one part DMSO with 1,100 mg/l p-hydroxycoumarin acid, and 0.003 parts 30% H_2O_2). After 1 min, signals were detected for 5 min in the dark (Gbox, Syngene).

Immunoprecipitation

HEK293T cells were seeded in 15 cm dishes at 7×10^6 cells per dish. After 24 h, the media was exchanged with full DMEM supplemented with 250 µM Bpa. Cells were transfected using PEI as described above with 17.5 µg pcDNA3.1_Arr2-D78TAG-2xStrep and 17.5 µg of pIRE4-Bpa. After 48 h, the cells were irradiated with UV light, as described above. The media was aspirated, and the cells were frozen at −80°C for 20–30 min and detached with 5 ml Triton lysis buffer 2 (20 mM Tris–HCl pH 7.4, 150 mM NaCl, 1% (v/v) Triton X-100, and 1× protease inhibitor) per dish. After an incubation of 30 min on ice with vortexing steps every 10 min, the cell debris was pelleted at 16,000 g for 45 min at 4°C. The supernatant was supplemented with NaCl and urea for a final concentration of 1 M each. Strep-Tactin-XT beads (IBA Lifesciences) were added to the supernatant (1 µl of resin, i.e., 2 µl slurry per 1 ml of supernatant) and incubated overnight at 4°C under constant gentle agitation. The sample was loaded on a 1 ml empty column equipped with a filter and washed five times with one column volume (CV) of buffer W (100 mM Tris–HCl pH 8.0, 150 mM NaCl, and 1 mM EDTA). Bound protein was eluted with 8 × 1 CV Buffer BXT (Buffer W supplemented with 50 mM biotin). Samples of the supernatant, flow-through, wash, and elution fractions were separated by SDS–PAGE and analyzed by Western blot, as described above. Membranes were blocked overnight in 1% BSA in TBS-T and incubated overnight at 4°C in α-Strep-tag antibody (IBA Lifesciences; 1:2,000 in blocking solution). Secondary antibody incubation with α-mouse-HRP and ECL detection was performed as described above. All fractions containing the protein of interest were pooled and concentrated to a total volume of 500 µl using a centrifugal concentrator with a 3K cutoff membrane (PALL) according to the manufacturer instructions.

Size exclusion chromatography

The purified crosslinked sample from the Strep-Tactin IP was applied to SEC. The SEC was performed at 4°C using ÄKTA advent system equipped with a Superdex 200 Increase 10/300 GL column (GE Healthcare). Buffer W was used as running buffer. For all steps the flowrate was set to 0.6 ml/min. The column was equilibrated with 1.5 CV of Buffer W. Absorbance was detected at 280 nm.

MALDI-TOF-MS

After SEC, protein samples were embedded in "super-DHB" matrix, a 9:1 (w/w) mixture of 2,5-dihydroxybenzoic acid and 2-hydroxy-5-methoxybenzoic acid, and analyzed via MALDI-TOF-MS (Ultraflex III, Bruker Daltonik, Bremen).

Nano-HPLC/Nano-ESI-Orbitrap-MS/MS

Samples from SEC were proteolyzed either by trypsin or a combination of trypsin and endoproteinase GluC with the SMART Digest trypsin kit (Thermo Fisher Scientific) following the manufacturer's protocol (1 h, 70°C). For the combined trypsin/GluC digestion, trypsin beads were removed after the tryptic digestion before GluC was added. Proteolysis was allowed to proceed for 2 h at 37°C. Then, cysteines were reduced with DTT and alkylated with iodoacetamide.

Samples were analyzed on an Ultimate 3000 RSLC nano-HPLC system coupled with an Orbitrap Q-Exactive Plus mass spectrometer (Thermo Fisher Scientific). Chromatography was performed by applying 90-min gradients with reversed phase C18 columns (µPAC 900 nl C18 trapping column and µPAC™ 50 cm C18 chip-based separation column, Pharmafluidics). For MS data acquisition, a data-dependent top 10 method was used. FTMS survey scans were performed in the m/z range 375–1,799, R = 140,000 at m/z 200, AGC (automated gain control) target value 3×10^6, and a maximum injection time of 100 ms. MS/MS scans were performed of the 10 most abundant signals of the survey scan with stepped higher energy collision-induced dissociation with 27, 30, and 33% normalized collision energy, quadrupole isolation window 2 Th, AGC target value 2×10^5, and maximum injection time 250 ms. Dynamic exclusion was enabled, and exclusion time was set to 60 s.

LC/MS data were processed with the Proteome Discoverer software, version 2.4 (Thermo Fisher Scientific). For peptide identification, MS/MS data were searched against the UniProt database (version Feb. 2019, taxonomy human, 73,801 entries, with sequence of arrestin-strep added) using Sequest HT with the following settings: Precursor mass error < 5 ppm, product ion mass error < 0.02 Da, variable modifications: Oxidation of Met, acetylation of protein N-termini, conversion of Asp to Bpa, fixed modification: carbamidomethylation of Cys, up to three missed cleavage sites. Peptides were filtered for false discovery rate < 1%.

Recruitment assay

Ligand-induced recruitment of βarr1/2 and their Bpa variants to PTH1R was assessed using the NanoBiT® complementation assay (Soave *et al*, 2020). The constructs for the assay were cloned as follows: PTH1R-LgBiT was cloned by inserting the ORF of the PTH1R into pBiT1.1-C using the restriction sites NheI and EcoRI. SmBiT-βarr1/2 were cloned by inserting the ORF of βarr1/2 in pBiT2.1-N between the restriction sites XhoI and NheI.

Ninety-six-well plates (Greiner) were precoated with poly-D-lysine (MW = 500–550 kDa) as described before (Serfling *et al*, 2018b). HEK293T cells were seeded at a density of 20,000 cells/well. After 24 h, half of the media was discarded and replaced with full DMEM supplemented with Bpa to a final concentration of 250 μM. The cells were transiently transfected with expression constructs for SmBit-βarr1/2-xxxTAG (50 ng), PTH1R-LgBit (50 ng), and pIRE4-Bpa (50 ng) using PEI as described above. After 48 h, the cells were washed with FluoroBrite media (Thermo Fisher Scientific) and subsequently kept in 100 μl FluoroBrite media (+10% FCS, 1× Pen/Strep). Twenty-five microliter per well of a 5× solution of the Nano-Glo® live cell reagent containing the cell-permeable furimazine substrate was added, and the baseline luminescence was immediately monitored for 15 min with 30-s intervals. The ligand PTH(1–34) was added to a final concentration of 200 nM, and luminescence was immediately monitored for 45 min with 30-s intervals. All luminescence measurements were performed using a FLUOstar Omega plate reader (BMG Labtech) at 37°C. Data analysis was performed using GraphPad Prism 5 (GraphPad Software).

Data availability

The mass spectrometry proteomics data have been deposited to the ProteomeXchange Consortium via the PRIDE (Perez-Riverol *et al*, 2019) partner repository with the dataset identifier PXD020418 (http://www.ebi.ac.uk/pride/archive/projects/PXD020418) and https://doi.org/10.6019/PXD020418.

Expanded View for this article is available online.

Author contributions
IC conceived and supervised the project. TB established the Bpa incorporation and crosslinking procedure, performed all crosslinking experiments, purified crosslinked products, performed preliminary MS analysis, performed part of the arrestin recruitment experiments, and synthesized BrEtY under the supervision of EB. SE performed the SEC purification and analysis; RS established the arrestin recruitment assays and performed part of recruitment experiments; CI performed MS analysis under the supervision of AS; and VVG participated to the conception of the project and provided material and advice. The manuscript was written by TB with the collaboration of SE and CI and was revised by IC and VVG.

Conflict of interest
The authors declare that they have no conflict of interest.

References

Boularan C, Scott MG, Bourougaa K, Bellal M, Esteve E, Thuret A, Benmerah A, Tramier M, Coppey-Moisan M, Labbe-Jullie C *et al* (2007) beta-arrestin 2 oligomerization controls the Mdm2-dependent inhibition of p53. *Proc Natl Acad Sci U S A* 104: 18061−18066

Cahill TJ 3rd, Thomsen AR, Tarrasch JT, Plouffe B, Nguyen AH, Yang F, Huang LY, Kahsai AW, Bassoni DL, Gavino BJ *et al* (2017) Distinct conformations of GPCR-beta-arrestin complexes mediate desensitization, signaling, and endocytosis. *Proc Natl Acad Sci U S A* 114: 2562−2567

Chen Q, Zhuo Y, Kim M, Hanson SM, Francis DJ, Vishnivetskiy SA, Altenbach C, Klug CS, Hubbell WL, Gurevich VV (2014) Self-association of arrestin family members. *Handb Exp Pharmacol* 219: 205−223

Chen Q, Perry NA, Vishnivetskiy SA, Berndt S, Gilbert NC, Zhuo Y, Singh PK, Tholen J, Ohi MD, Gurevich EV *et al* (2017) Structural basis of arrestin-3 activation and signaling. *Nat Commun* 8: 1427

Chin JW, Cropp TA, Anderson JC, Mukherji M, Zhang Z, Schultz PG (2003) An expanded eukaryotic genetic code. *Science* 301: 964−967

Coffa S, Breitman M, Hanson SM, Callaway K, Kook S, Dalby KN, Gurevich VV (2011) The effect of arrestin conformation on the recruitment of c-Raf1, MEK1, and ERK1/2 activation. *PLoS ONE* 6: e28723

Coin I, Perrin MH, Vale WW, Wang L (2011) Photo-cross-linkers incorporated into G-protein-coupled receptors in mammalian cells: a ligand comparison. *Angew Chem Int Ed Engl* 50: 8077−8081

Coin I, Katritch V, Sun T, Xiang Z, Siu FY, Beyermann M, Stevens RC, Wang L (2013) Genetically encoded chemical probes in cells reveal the binding path of urocortin-I to CRF class B GPCR. *Cell* 155: 1258−1269

Coin I (2018) Application of non-canonical crosslinking amino acids to study protein-protein interactions in live cells. *Curr Opin Chem Biol* 46: 156−163

Dorman G, Prestwich GD (1994) Benzophenone photophores in biochemistry. *Biochemistry* 33: 5661−5673

Eichel K, Jullié D, von Zastrow M (2016) β-Arrestin drives MAP kinase signalling from clathrin-coated structures after GPCR dissociation. *Nature Cell Biol* 18: 303−310

Gagnon L, Cao Y, Cho A, Sedki D, Huber T, Sakmar TP, Laporte SA (2019) Genetic code expansion and photocross-linking identify different beta-arrestin binding modes to the angiotensin II type 1 receptor. *J Biol Chem* 294: 17409−17420

Goodman OB Jr, Krupnick JG, Santini F, Gurevich VV, Penn RB, Gagnon AW, Keen JH, Benovic JL (1996) Beta-arrestin acts as a clathrin adaptor in endocytosis of the beta2-adrenergic receptor. *Nature* 383: 447–450

Grammatopoulos DK (2012) Insights into mechanisms of corticotropin-releasing hormone receptor signal transduction. *Br J Pharmacol* 166: 85–97

Gurevich EV, Benovic JL, Gurevich VV (2004) Arrestin2 expression selectively increases during neural differentiation. *J Neurochem* 91: 1404–1416

Gurevich VV, Dion SB, Onorato JJ, Ptasienski J, Kim CM, Sterne-Marr R, Hosey MM, Benovic JL (1995) Arrestin interactions with G protein-coupled receptors. Direct binding studies of wild type and mutant arrestins with rhodopsin, beta 2-adrenergic, and m2 muscarinic cholinergic receptors. *J Biol Chem* 270: 720–731

Gurevich VV, Gurevich EV (2006) The structural basis of arrestin-mediated regulation of G-protein-coupled receptors. *Pharmacol Ther* 110: 465–502

Gurevich VV (2014) Arrestins: pharmacology and therapeutic potential. In *Handbook of Experimental Pharmacology 219*, Gurevich VV (ed), pp. VIII, 447. Berlin, Heidelberg: Springer-Verlag.

Han M, Gurevich VV, Vishnivetskiy SA, Sigler PB, Schubert C (2001) Crystal structure of beta-arrestin at 1.9 A: possible mechanism of receptor binding and membrane translocation. *Structure* 9: 869–880

Hanson SM, Vishnivetskiy SA, Hubbell WL, Gurevich VV (2008) Opposing effects of inositol hexakisphosphate on rod arrestin and arrestin2 self-association. *Biochemistry* 47: 1070–1075

Huang W, Masureel M, Qianhui Q, Janetzko J, Inoue A, Kato HE, Robertson MJ, Nguyen KC, Glenn JS, Skiniotis G et al (2020) Structure of the neurotensin receptor 1 in complex with beta-arrestin 1. *Nature* 579: 303–308

Jones KT, Echeverry M, Mosser VA, Gates A, Jackson DA (2006) Agonist mediated internalization of M2 mAChR is beta-arrestin-dependent. *J Mol Signal* 1: 7

Kang Y, Zhou XE, Gao X, He Y, Liu W, Ishchenko A, Barty A, White TA, Yefanov O, Han GW et al (2015) Crystal structure of rhodopsin bound to arrestin by femtosecond X-ray laser. *Nature* 523: 561–567

Kaya AI, Perry NA, Gurevich VV, Iverson TM (2020) Phosphorylation barcode-dependent signal bias of the dopamine D1 receptor. *Proc Natl Acad Sci U S A* 117: 14139–14149

Lang K, Nguyen TA, Cigler M (2018) Expanding the genetic code to study protein-protein interactions. *Angew Chem Int Ed Engl* 57: 14350–14361

Laporte SA, Oakley RH, Zhang J, Holt JA, Ferguson SS, Caron MG, Barak LS (1999) The beta2-adrenergic receptor/betaarrestin complex recruits the clathrin adaptor AP-2 during endocytosis. *Proc Natl Acad Sci U S A* 96: 3712–3717

Lee Y, Warne T, Nehmé R, Pandey S, Dwivedi-Agnihotri H, Chaturvedi M, Edwards PC, García-Nafría J, Leslie AGW, Shukla AK et al (2020) Molecular basis of β-arrestin coupling to formoterol-bound β1-adrenoceptor. *Nature* 583: 862–866

Luttrell LM, Lefkowitz RJ (2002) The role of beta-arrestins in the termination and transduction of G-protein-coupled receptor signals. *J Cell Sci* 115: 455–465

Mayer D, Damberger FF, Samarasimhareddy M, Feldmueller M, Vuckovic Z, Flock T, Bauer B, Mutt E, Zosel F, Allain FHT et al (2019) Distinct G protein-coupled receptor phosphorylation motifs modulate arrestin affinity and activation and global conformation. *Nat Commun* 10: 1261

Milano SK, Kim YM, Stefano FP, Benovic JL, Brenner C (2006) Nonvisual arrestin oligomerization and cellular localization are regulated by inositol hexakisphosphate binding. *J Biol Chem* 281: 9812–9823

Nguyen AH, Thomsen ARB, Cahill TJ 3rd, Huang R, Huang LY, Marcink T, Clarke OB, Heissel S, Masoudi A, Ben-Hail D et al (2019) Structure of an endosomal signaling GPCR-G protein-beta-arrestin megacomplex. *Nat Struct Mol Biol* 26: 1123–1131

Nobles KN, Xiao K, Ahn S, Shukla AK, Lam CM, Rajagopal S, Strachan RT, Huang TY, Bressler EA, Hara MR et al (2011) Distinct phosphorylation sites on the beta(2)-adrenergic receptor establish a barcode that encodes differential functions of beta-arrestin. *Sci Signal* 4: ra51

Oakley RH, Laporte SA, Holt JA, Barak LS, Caron MG (1999) Association of beta-arrestin with G protein-coupled receptors during clathrin-mediated endocytosis dictates the profile of receptor resensitization. *J Biol Chem* 274: 32248–32257

Oakley RH, Laporte SA, Holt JA, Caron MG, Barak LS (2000) Differential affinities of visual arrestin, beta arrestin1, and beta arrestin2 for G protein-coupled receptors delineate two major classes of receptors. *J Biol Chem* 275: 17201–17210

Oakley RH, Laporte SA, Holt JA, Barak LS, Caron MG (2001) Molecular determinants underlying the formation of stable intracellular G protein-coupled receptor-beta-arrestin complexes after receptor endocytosis*. *The Journal of biological chemistry* 276: 19452–19460

Oakley RH, Olivares-Reyes JA, Hudson CC, Flores-Vega F, Dautzenberg FM, Hauger RL (2007) Carboxyl-terminal and intracellular loop sites for CRF1 receptor phosphorylation and beta-arrestin-2 recruitment: a mechanism regulating stress and anxiety responses. *Am J Physiol Regul Integr Comp Physiol* 293: R209–R222

Perez-Riverol Y, Csordas A, Bai J, Bernal-Llinares M, Hewapathirana S, Kundu DJ, Inuganti A, Griss J, Mayer G, Eisenacher M et al (2019) The PRIDE database and related tools and resources in 2019: improving support for quantification data. *Nucleic Acids Res* 47: D442–D450

Schwarz R, Tanzler D, Ihling CH, Muller MQ, Kolbel K, Sinz A (2013) Monitoring conformational changes in peroxisome proliferator-activated receptor alpha by a genetically encoded photoamino acid, cross-linking, and mass spectrometry. *J Med Chem* 56: 4252–4263

Schwarz R, Tanzler D, Ihling CH, Sinz A (2016) Monitoring solution structures of peroxisome proliferator-activated receptor beta/delta upon ligand binding. *PLoS ONE* 11: e0151412

Seidel L, Zarzycka B, Zaidi SA, Katritch V, Coin I (2017) Structural insight into the activation of a class B G-protein-coupled receptor by peptide hormones in live human cells. *Elife* 6: e27711

Seidel L, Zarzycka B, Katritch V, Coin I (2019) Exploring pairwise chemical crosslinking to study peptide-receptor interactions. *ChemBioChem* 20: 683–692

Serfling R, Coin I (2016) Incorporation of unnatural amino acids into proteins expressed in mammalian cells. *Methods Enzymol* 580: 89–107

Serfling R, Lorenz C, Etzel M, Schicht G, Bottke T, Morl M, Coin I (2018a) Designer tRNAs for efficient incorporation of non-canonical amino acids by the pyrrolysine system in mammalian cells. *Nucleic Acids Res* 46: 1–10

Serfling R, Seidel L, Bottke T, Coin I (2018b) Optimizing the genetic incorporation of chemical probes into GPCRs for photo-crosslinking mapping and bioorthogonal chemistry in live mammalian cells. *J Vis Exp* 134: 57069

Shiina T, Kawasaki A, Nagao T, Kurose H (2000) Interaction with beta-arrestin determines the difference in internalization behavor between beta1- and beta2-adrenergic receptors. *J Biol Chem* 275: 29082–29090

Shukla AK, Westfield GH, Xiao K, Reis RI, Huang LY, Tripathi-Shukla P, Qian J, Li S, Blanc A, Oleskie AN et al (2014) Visualization of arrestin recruitment by a G-protein-coupled receptor. *Nature* 512: 218–222

Shukla AK, Dwivedi-Agnihotri H (2020) Structure and function of beta-arrestins, their emerging role in breast cancer, and potential opportunities for therapeutic manipulation. *Adv Cancer Res* 145: 139–156

Soave M, Kellam B, Woolard J, Briddon SJ, Hill SJ (2020) NanoBiT complementation to monitor agonist-induced adenosine A1 receptor internalization. *SLAS Discov* 25: 186−194

Song X, Coffa S, Fu H, Gurevich VV (2009) How does arrestin assemble MAPKs into a signaling complex? *J Biol Chem* 284: 685−695

Staus DP, Hu H, Robertson MJ, Kleinhenz ALW, Wingler LM, Capel WD, Latorraca NR, Lefkowitz RJ, Skiniotis G (2020) Structure of the M2 muscarinic receptor-beta-arrestin complex in a lipid nanodisc. *Nature* 579: 297−302

Sun D, Ostermaier MK, Heydenreich FM, Mayer D, Jaussi R, Standfuss J, Veprintsev DB (2013) AAscan, PCRdesign and MutantChecker: a suite of programs for primer design and sequence analysis for high-throughput scanning mutagenesis. *PLoS ONE* 8: e78878

Szczepek M, Beyriere F, Hofmann KP, Elgeti M, Kazmin R, Rose A, Bartl FJ, von Stetten D, Heck M, Sommer ME *et al* (2014) Crystal structure of a common GPCR-binding interface for G protein and arrestin. *Nat Commun* 5: 4801

Thomsen AR, Plouffe B, Cahill TJ 3rd, Shukla AK, Tarrasch JT, Dosey AM, Kahsai AW, Strachan RT, Pani B, Mahoney JP *et al* (2016) GPCR-G protein-beta-arrestin super-complex mediates sustained G protein signaling. *Cell* 166: 907−919

Tobin AB, Butcher AJ, Kong KC (2008) Location, location, location..site-specific GPCR phosphorylation offers a mechanism for cell-type-specific signalling. *Trends Pharmacol Sci* 29: 413−420

Vilardaga JP, Krasel C, Chauvin S, Bambino T, Lohse MJ, Nissenson RA (2002) Internalization determinants of the parathyroid hormone receptor differentially regulate beta-arrestin/receptor association. *J Biol Chem* 277: 8121−8129

Vishnivetskiy SA, Hosey MM, Benovic JL, Gurevich VV (2004) Mapping the arrestin-receptor interface. Structural elements responsible for receptor specificity of arrestin proteins. *J Biol Chem* 279: 1262−1268

Vishnivetskiy SA, Gimenez LE, Francis DJ, Hanson SM, Hubbell WL, Klug CS, Gurevich VV (2011) Few residues within an extensive binding interface drive receptor interaction and determine the specificity of arrestin proteins. *J Biol Chem* 286: 24288−24299

Wang L (2017a) Engineering the genetic code in cells and animals: biological considerations and impacts. *Acc Chem Res* 50: 2767−2775

Wang L (2017b) Genetically encoding new bioreactivity. *N Biotechnol* 38: 16−25

Wehbi VL, Stevenson HP, Feinstein TN, Calero G, Romero G, Vilardaga JP (2013) Noncanonical GPCR signaling arising from a PTH receptor-arrestin-Gbetagamma complex. *Proc Natl Acad Sci U S A* 110: 1530−1535

Xiang Z, Ren H, Hu YS, Coin I, Wei J, Cang H, Wang L (2013) Adding an unnatural covalent bond to proteins through proximity-enhanced bioreactivity. *Nat Methods* 10: 885−888

Xiang Z, Lacey VK, Ren H, Xu J, Burban DJ, Jennings PA, Wang L (2014) Proximity-enabled protein crosslinking through genetically encoding haloalkane unnatural amino acids. *Angew Chem Int Ed Engl* 53: 2190−2193

Xiao K, McClatchy DB, Shukla AK, Zhao Y, Chen M, Shenoy SK, Yates JR 3rd, Lefkowitz RJ (2007) Functional specialization of beta-arrestin interactions revealed by proteomic analysis. *Proc Natl Acad Sci U S A* 104: 12011−12016

Yang F, Yu X, Liu C, Qu CX, Gong Z, Liu HD, Li FH, Wang HM, He DF, Yi F *et al* (2015) Phospho-selective mechanisms of arrestin conformations and functions revealed by unnatural amino acid incorporation and (19)F-NMR. *Nat Commun* 6: 8202

Yang B, Tang S, Ma C, Li ST, Shao GC, Dang B, DeGrado WF, Dong MQ, Wang PG, Ding S *et al* (2017) Spontaneous and specific chemical cross-linking in live cells to capture and identify protein interactions. *Nat Commun* 8: 2240

Yin W, Li Z, Jin M, Yin YL, de Waal PW, Pal K, Yin Y, Gao X, He Y, Gao J *et al* (2019) A complex structure of arrestin-2 bound to a G protein-coupled receptor. *Cell Res* 29: 971−983

Zhan X, Gimenez LE, Gurevich VV, Spiller BW (2011) Crystal structure of arrestin-3 reveals the basis of the difference in receptor binding between two non-visual subtypes. *J Mol Biol* 406: 467−478

Zhao LH, Ma S, Sutkeviciute I, Shen DD, Zhou XE, de Waal PW, Li CY, Kang Y, Clark LJ, Jean-Alphonse FG *et al* (2019) Structure and dynamics of the active human parathyroid hormone receptor-1. *Science* 364: 148−153

Zhou XE, He Y, de Waal PW, Gao X, Kang Y, Van Eps N, Yin Y, Pal K, Goswami D, White TA *et al* (2017) Identification of phosphorylation codes for arrestin recruitment by G protein-coupled receptors. *Cell* 170: 457−469.e413